Published in Chemical Physics 233, 207 (1998)

Controlling Condensed Phase Vibrational Excitation with Tailored Infrared Pulses

V. D. Kleiman,[#] S. M. Arrivo,[*] and E. J. Heilweil

Optical Technology Division, National Institute of Standards and Technology, Gaithersburg, MD 20899

J. S. Melinger

Condensed Matter and Radiation Sciences Division, Naval Research Laboratory, Washington, DC 20375

Abstract

Vibrational population distributions within the CO-stretching T_{1u} manifold of $W(CO)_6$ in room temperature n-hexane were created by using near transform-limited and linearly chirped picosecond infrared excitation pulses. These pulses were characterized using the second harmonic FROG (frequency-resolved optical gating) algorithm to determine the ca. 8 cm^{-1}/ps chirp for both positively and negatively chirped 2 ps pulses. FROG and time-resolved transient difference spectra were obtained with an InSb focal plane array detector. While unchirped and positively chirped excitation leads predominantly to v=1 population, negatively chirped pulses produce excess population in the v=2 level. These results are compared to predictions from density matrix calculations for a model potential.

INTRODUCTION

The notion of directly altering and controlling vibrational population by using specifically designed excitation pulses has become the center of increasing attention[1-5]. Under routine situations, excitation is accomplished with near-transform limited (all frequency components of the pulse arrive at the sample simultaneously) infrared (IR) picosecond or femtosecond pulses. However, since polyatomic electronic ground state vibrational potential energy surfaces are generally anharmonic, it is possible that non-transform limited pulses may enhance or hinder final state distributions of a multiphoton excitation processes. Since ultrashort pulse-shaping and pulse-analysis techniques are now widely used, a whole new approach to studying and affecting vibrational dynamics on ground electronic state potential energy surfaces (PES) has become available. By appropriately controlling the arrival time of different frequency components of an IR

[#] Guest Researcher from Dept of Chemical Engineering, UCLA.
[*] Current Address: Merck and Company, Inc. WP38-3, P.O. Box 4, Westpoint, PA 19486

excitation pulse, for example, one can in principle readily transfer and "control" excited state population in otherwise inaccessible regions of the PES. Comparing measured population dynamics (produced by using carefully chosen and characterized experimental pulse parameters) to theoretical calculations could then lead to better analytical models for potential surfaces of complex systems.

There are two broad-based schemes for accessing vibrationally excited ground electronic state surfaces via coherent control. One involves multiphoton excitation through an excited electronic state (i.e. Impulsive Raman-excitation with chirped visible pulses [6,7], stimulated Raman adiabatic passage (STIRAP) [8]). In this case, interpretation of the results involves detailed knowledge of the dynamics on excited electronic surfaces. Another possibility is through direct multiphoton "climbing" of a vibrational mode overtone ladder using phase-modulated IR excitation pulses (see below). This latter method requires prior knowledge of only ground electronic state parameters (vibrational state lifetimes, IR cross-sections, state-to-state couplings, etc.) for interpreting prepared population distributions.

Ultrafast pulses are advantageous for inducing and probing photochemical reactions on timescales shorter or comparable to those of competing relaxation or emission processes. In addition, when excitation schemes involving the coherent properties of the states are employed, interferences can be beneficially used to manipulate the final product state distribution [9]. In the case of vibrational populations, for example, state-selective distributions can be obtained by constructive or destructive interference between different components of the excited wavefunction. Therefore, it may be possible to affect efficient mode-specific chemical bond-breaking reactions in ground electronic state molecules using properly tailored ultrafast infrared pulses.

There are a number of theoretical predictions for phase-controlled multiphoton infrared excitation that have yet to be experimentally explored or verified. Just et. al. [2] modeled the IR excitation of gas phase OH radicals and found that a linear chirp imposed on a $\sin^2$ pulse envelope could transfer population to higher vibrational levels if state selectivity was not required. A similar result was found by Paramonov [5] where optimization of the pulse amplitude and pulse timing sequence improved the population selectivity on the final state. That work was extended by Korolkov et. al. to include preparation of high lying states that could lead to dissociation in diatomic molecules [3]. Melinger, et. al. [4] explored the use of single pulses with amplitude and phase modulation to invert vibrational populations. In that work, the robustness of the control for different pulse parameters was examined. While all of the calculations mentioned above were performed for model "isolated" diatomics or single mode oscillators, condensed-phase systems usually contain complex coupling mechanisms to the bath, as well as couplings of the vibrational modes within the molecule. For the work presented here, we consider these theoretical models as zeroth order approximations to the anharmonic vibrational overtone excitations that are possible in the condensed-phase when ultrashort IR pulses are employed.

Recently, there has been an increasing number of experiments which applied coherent control methods. Control of the dynamics of an electronically excited wave-packet has been shown to occur in the gas phase [10] and in matrices by [11]. Experiments aimed at modifying ground electronic state dynamics with chirped pulses

have been performed using visible pulses interacting with electronic excited states [6,12]. Adiabatic rapid passage has also been used to control excitation of atomic systems. For example, both the chirp direction and field strength of an ultrashort pulse were used to alter the population transferred from the 5s to the 5d state in Rubidium atoms [13,14]. While negatively chirped pulses (red frequencies arriving after blue frequencies) increased the population transfer by 100%, positively chirped pulses (red frequencies arriving before blue frequencies) inhibited the process. The use of unchirped IR pulses to climb a single oscillator vibrational ladder was recently reported for gas phase NO [15] and $W(CO)_6$ in the liquid phase [16].

We present in this paper the first known experimental results which demonstrate control of the vibrational state population distribution in a multibond, polyatomic condensed-phase system using tailored picosecond IR excitation pulses. Specifically, we re-investigated multiphoton vibrational excitation of $W(CO)_6$ in room temperature n-hexane solution [16] but we now use deliberately chirped IR pulses. We show how specific phase properties of an IR excitation pulse alter the vibrational population distribution within a molecular mode vibrational ladder. These results suggest the possibility of creating a desired excited vibrational state population distribution or potentially populating dissociative overtone states by proper choice of excitation pulse parameters. In the first section we explain how IR pulses are produced and analyzed. We then give a brief overview of theoretical calculations using experimentally determined pulse parameters which model the results. Finally, these results are discussed in terms of potential future applications.

EXPERIMENTAL

Broadband IR Spectrometer

Infrared excitation (pump) and probe pulses were obtained by difference frequency generation (DFG) between two amplified picosecond synchronously-pumped dye lasers [16]. The pulsed output of the R6G dye laser (589 nm, autocorrelation 0.9 ps FWHM) was stretched by passage through a 30 cm long optical fiber producing 2-4 ps broadband pulses. These pulses were amplified (in three-stage dye amplifiers pumped by the second harmonic of a 20 Hz Nd:YAG regenerative-amplifier) to approximately 800 μJ and beamsplit to generate independent pump and probe IR beams. After amplification, the visible pulses were compressed with a double pass grating-compressor and then combined with 7 ps, 60 μJ pulses from a similarly amplified DCM synch-pumped dye laser in a 5 mm long $LiIO_3$ crystal to generate broadband IR pulses centered at 5 μm (ca. 40 nJ/pulse). The $LiIO_3$ crystal was tuned off-phase matching to provide broadband IR probe and reference pulses with >100 cm^{-1} spectral coverage near 1960 cm^{-1} [17]. Pump pulses were similarly produced (via DFG) with a 20 mm long $LiIO_3$ crystal yielding 0.2-0.4 μJ energy. Pulse chirping details are described in the next section.

Pump and probe beams were coincidentally focused to a ~100 μm diameter spot and overlapped in a 1 mm thick CaF_2 flow cell containing a $W(CO)_6$ in hexane solution (OD ~1). After traversing the cell, the probe and reference beams were dispersed by a

30 cm (f/4) IR monochromator onto a 256x256 element (30 micron pixel spacing) InSb IR Focal Plane Array camera [17]. The horizontal dimension of the detector (corresponding to spectral frequency) yielded a 0.88 cm^{-1}/pixel dispersion primarily governed by the 70 groove/mm grating of the monochromator. The imaged probe and reference beams were 25 pixels high and separated by 50 pixels. Our data acquisition software vertically integrates each beam and ratios the probe and reference spectra on each laser shot (normalization for large amplitude and frequency fluctuations) for pump-on/pump-off conditions. By averaging 4000 laser shots, transient IR absorption difference spectra are readily measured ($\Delta OD > 0.005$) in a matter of minutes with 6 cm^{-1} FWHM spectral resolution at variable picosecond time delays.

Generation of Chirped Infrared Excitation Pulses

Positively and negatively chirped IR pump pulses were derived by DFG between picosecond DCM pulses and deliberately chirped R6G pulses. To produce positively chirped IR pulses, a 50% beam-splitter was placed directly after the R6G dye laser amplifier chain. The amplified fiber output (before the compressor) carries a strong positive group velocity chirp that is transferred to the generated IR pulse during the DFG process. As was also the case for negatively chirped pulses, a SHG-FROG measurement was performed on these generated positively-chirped IR pulses to extract an average linear chirp coefficient before they were used in the up-pumping experiment.

Negatively-chirped pump pulses were produced by positioning the 50% RG6 beam splitter after the compressor and increasing the compressor length. The double-pass compressor was composed of a 333 grooves/mm grating blazed for 600 nm (82% reflectivity at Littrow angle). At a grating to retro-reflector separation distance of ca. 40 cm, optimum compression and near-transform limited 80 Mhz or amplified pulses of ca. 100 fs FWHM are obtained. By lengthening the compressor grating-mirror distance to 70 cm, the pulsewidth increased to about 1 ps FWHM and the pulse becomes negatively chirped [18]. The compressor output (50 % throughput) is then split equally and used to generate the pump and probe pulses via the two $LiIO_3$ crystals described above.

"Standard" transform-limited IR pump pulses (~300 nJ/pulse) were obtained by DFG between amplified DCM pulses and the optimally compressed output of the R6G dye laser. Previous experiments conducted in this laboratory have shown that when mixing a ~100 fs compressed yellow pulse with a "long" DCM pulse, a transform-limited IR pulse of about 1 ps FWHM and ~10 cm^{-1} FWHM bandwidth is produced. Although we did not perform a SHG-FROG or autocorrelation measurement on these pulses, we did measure a pulse spectral bandwidth of 13 cm^{-1} FWHM which corresponds to a ~1 ps $sech^2$ pulsewidth.

Difference frequency generation of the three types of pump pulses was performed in a 20 mm long $LiIO_3$ crystal under optimized phase-matching conditions. For this pulse generating method, it is important to consider the possibility of frequency and temporal dispersion that the $LiIO_3$ crystal could impose on different IR pulses. By using the appropriate Sellmeier equation for the ordinary and extraordinary indices of refraction for $LiIO_3$ [19], we evaluated the difference in propagation times for all input and output wavelengths. Although the two visible pulses experience very different propagation

times ($\Delta t \approx 455$ fs/mm) the calculation predicts no appreciable difference between the R6G and IR pulse transient propagation times ($\Delta t < 1$ fs/mm). Under these conditions, we infer that the phase properties of the shaped input R6G pulse are directly transferred without significant distortion to the generated IR pulse.

Infrared Pump Pulse SHG-FROG Analysis

If we can assume that the DFG crystal does not substantially change the chirp properties carried by the R6G pulse, the chirp magnitude and sign will be directly imposed onto the generated IR pulse. Since this situation is atypical, we elected to directly measure the E(t) field and instantaneous frequency of the chirped IR pump pulses using SHG-Frequency Resolved Optical Gating [20]. Briefly, the SHG-FROG technique consists of spectrally resolving the second-harmonic output of the mid-IR pulse time-dependent autocorrelation function. For our purposes, the pump output was split into two beams with one of them sent through a variable delay line before being overlapped with the other beam and focused (10 cm CaF_2 lens) in an off-axis SHG autocorrelation crystal (1 cm $LiIO_3$). The 2.5 μm SHG output was collected and dispersed by the same IR grating monochromator (in 2^{nd} order) and detected with the IR-FPA. An averaged pulse spectrum (2000 shots) is collected for each delay time between the interferometer arms and the time-frequency information is stored in a PC. The FROG trace for the positively-chirped pulses was constructed with 65 time delays (21.5 ps across the complete scan) and 247 wavelengths (covering ca. 240 nm). The negatively-chirped pulse (sampled at a higher temporal resolution) encompassed 81 time steps (13.5 ps scan) and 245 wavelengths. Since the amplified dye laser system generates IR pulses with highly fluctuating pulse-to-pulse amplitude and frequency components, an average of many pulses is required to generate a FROG trace. Approximately 2000 shots were averaged for each spectrum, thus taking more than 2 hrs to collect the full FROG trace. The average power of the generated 5 μm pulses was simultaneously recorded for normalization purposes although this proved to be unnecessary since the largest source of error arises from spectral fluctuations and not integrated power. The original 5 μm pulse electric-field amplitude and phase were reconstructed from the time-spectral data using the phase retrieval algorithm developed by Kane and Trebino [20] (supplied by Femtosoft Technology).[†]

CHIRPED-PULSE EXCITATION MODELLING

Population excitation of a manifold of overtone vibrational states was modelled using the density matrix formalism which we then solved numerically. Briefly, the model incorporates a Morse oscillator manifold of anharmonic vibrational levels (v=0 to 10 with constant 15 cm^{-1} anharmonicity [16] and fixed absorption dipole moment of 1 Debye) but does not include other cross-manifold relaxation channels. For $W(CO)_6$ in solution, there are indeed other CO-stretching modes and IR-inactive states which could couple to the

[†] Commercial equipment and software is identified but in no case does such identification imply recommendation or endorsement by NIST.

strongly IR-allowed T_{1u} manifold studied here. However, since the measured population lifetimes for the v=1-3 levels ranges from 140 ps to 35 ps, respectively, for $W(CO)_6$ in n-hexane [16] and coupling to the higher-lying E_g level occurs within 25 ps [21], we assume that the present model is appropriate for excitation pulses of 1 to 2 ps duration.

One should also incorporate the coherence lifetimes between the interacting vibrational states. At present, the 5 cm^{-1} FWHM v=0→1 absorption indicates the T_2 coherence lifetime is approximately 3-4 ps: only a factor of 2-4 longer than our pump pulse durations. One might also expect the excited state coherence lifetimes to decrease with increasing quantum number (and increasing bandwidth), but our earlier transient absorption spectra for v=1→2, v=2→3 and v=3→4 show that minimal broadening occurs for these level transitions (T_2 does not change appreciably with n). At this point we have not incorporated excited state coherence lifetimes into the modelling.

For the purposes of this work, we modeled the pump pulse electric field with a Gaussian envelope function possessing linear up-chirp, down-chirp, or no chirp (transform limited). Pulse durations (FWHM), bandwidths and energies were input from the independently measured pulse characteristics described above. From these input vibrational state and pulse properties, the computer model predicts the relative ground and excited state vibrational populations as a function of peak Rabi frequency. The model does not currently include subsequent population relaxation processes or correction for intensity changes in the pump pulse spatial (radial) dimension. Future refinements of the model should reflect independently measured excited state coherence lifetimes, population relaxation to lower-lying states and other vibrations, and incorporate the excitation pulse field envelope and phase information directly extracted from the FROG algorithm.

RESULTS AND DISCUSSION

Figure 1 shows the FROG-retrieved time-dependent intensity profiles and temporal phases of the IR excitation pulses used in this experiment. The top panel corresponds to the negatively chirped pulse and the lower panel to the positively chirped IR excitation pulse. In each panel, the inset displays a comparison between the autocorrelation obtained experimentally and one derived from the retrieved pulse. Both pulses exhibit similar widths (approx. 2 psec FWHM) and chirp parameters (phase parabolic curvature). The structure seen in the negative-chirped pulse has a 350-500 fs period (corresponding to a 30-40 cm^{-1} spectral oscillation). This structure is not as pronounced in the positive-chirped pulse amplitude because the FROG trace was collected at half the temporal resolution.

The spectral profiles of the excitation pulses are obtained by Fourier transforming the temporal profiles in Fig.1. These transformations are shown in Figure 2 with the top panel representing the negatively-chirped pulse spectrum and the bottom panel corresponding to the positive chirp case. The dotted spectrum shown in the top panel is a direct measurement of the 5μm pulse spectrum obtained from the spectrometer-focal plane detector. As expected, the reconstructed spectra contain oscillations corresponding to the derived temporal structure, but these oscillations are not observed in the experimental spectrum. The source of the oscillations is not presently understood, but a

possible rationale is that they arise from fluctuations in the frequency domain of the amplified R6G pulse (e.g., from self-phase modulation in the optical fiber). When we acquire and average multiple IR pulse spectra, the high frequency structure observed for individual pulses is washed out by frequency shifts and the relatively low resolution of the spectrometer (ca. 10 cm^{-1} FWHM). Perhaps those oscillations are more precisely recorded in the time domain because of the higher resolution time step used for the negatively-chirped pulse measurement.

Figures 1 and 2 indicate that overall, both the up- and down-chirped pulses have similar time duration (ca. 2 ps FWHM), comparable spectral bandwidths (10-20 cm^{-1} FWHM) and chirp rate (second order parabolic curvature). The most significant difference between these two pulse types is the direction of change (sign) of their instantaneous frequency. To assess the instantaneous frequency we look at the temporal phase retrieved by the phase retrieval algorithm. The best fit to the extracted temporal phase is a quadratic function with a 7 cm^{-1}/ps chirp coefficient for the positively-chirped pulse and 8 cm^{-1}/psec for the negative-chirp case (solid lines in Figs 1 and 2). The extracted pulse phase functions are only shown and fit for the highest intensity regions of the pulses since outside these regions there is insufficient intensity and increasing uncertainty. The main disadvantage of the SHG-FROG geometry is the ambiguity in determining the temporal chirp direction. In this work, the chirp sign is fully determined from the DFG process used to generate the pulses. As discussed previously in the Experimental section, the R6G fiber optic stretcher imposes a well defined positive linear chirp on the amplified pulses while the deliberately elongated compressor imposes negative chirp on the generated IR pulse. These signs were incorporated in the FROG output to generate the results shown in Figs. 1 and 2.

Tungsten hexacarbonyl vibrational dynamics in solution has been extensively studied in the mid-IR region [21,16 and references therein]. For studying the effect of excitation pulse properties on overtone state distributions, we considered the strong IR-active T_{1u} mode (μ=1D with $v=0\rightarrow1$ transition at 1982 cm^{-1}) which corresponds to a triply degenerate antisymmetric CO-stretching motion. Arrivo et al [16] showed that with IR excitation, the vibrational excited state transient spectrum of $W(CO)_6$ strongly depends on the central frequency of the pumping pulse. As the maximum of the excitation pulse is red-shifted from the $v=0\rightarrow1$ transition frequency to the $v=1\rightarrow2$ transition frequency (near 1963 cm^{-1}), higher vibrational overtones are populated (as long as overlap between the pump spectrum and the $v=0\rightarrow1$ transition occurs). To avoid any uncertainties from excitation center wavelength for the present experiment, we only compare spectra that were collected with central frequency $\nu_{pump} > 1975$ cm^{-1}. A similar argument holds for the time delay between pump and probe pulses. In ref. [16] overtone population relaxation was observed as time-dependent amplitude changes in the transient absorption spectra. In the current case, we fixed the time delay between pump and probe pulses to guarantee that excited state relaxation dynamics did not confuse the comparison between spectra produced by different excitation pulses. We chose a fixed time delay of 40 ps to maximize absorption signals from the lower $v=1\rightarrow2$ and $v=2\rightarrow3$ transitions without completely suppressing the upper state population from the previously observed T_{1u} manifold cascading relaxation mechanism (see ref. [16]). By looking at long time delay,

we ensure that the probed population spectra are the net result of interference between the coherent properties of the states and excitation pulses after all coherences have damped.

The IR transient absorption vibrational spectrum resulting from up-pumping of the tungsten-hexacarbonyl CO-stretch manifold by a transform limited IR pulse (ca. 300 nJ/pulse) is shown in Figure 3 (middle panel). Removal of population from the v=0 ground state produces a bleach in the transient absorption spectrum centered at 1982 cm^{-1} (the full band is not shown but it reaches a maximum $\Delta OD=0.15$). Two new absorption features centered at 1967 cm^{-1} and 1952 cm^{-1} are generated with IR excitation and they are assigned to the $v = 1 \rightarrow 2$ and $v = 2 \rightarrow 3$ overtone absorptions, respectively. The transient absorption for the $v=1\rightarrow2$ transition produces an absorption change of $\Delta OD = 0.11$ while the $v = 2 \rightarrow 3$ absorption maximum is $\Delta OD = 0.025$. At 40 ps pump-probe time delay we do not expect to observe any $v = 3 \rightarrow 4$ absorption since the $v = 3$ population relaxation lifetime is 30±15 ps and there is minimal pump pulse spectral content at 1937 cm^{-1} to create significant v=3 population.

Figure 3 also depicts the transient difference spectra obtained with positively chirped (top) and negatively chirped (bottom) pump pulse excitation. The lower panel does not include the bleach ($v=0\rightarrow1$ transition) because the broadband probe was tuned to interrogate the longer wavelength (<1970 cm^{-1}) range. The striking difference between the transient IR spectra for the three types of excitation pulses is the amount of population produced in the v=2 state compared to the v=1 population. The effect of positive chirp excitation is readily seen as an almost completely diminished absorption at the $v = 2 \rightarrow 3$ transition (at 1950 cm^{-1}). This can be the result of having minimal population transfer to the v=2 state or having nearly equal populations in both the v=2 and v=3 levels. We dismiss the latter case since we would then anticipate observing $v=3\rightarrow4$ absorption in the transient spectrum (no red-shifted absorption was observed). On the other hand, down-chirped pulse excitation clearly enhances the up-pumping process by transferring most of the population to the highest accessible v=2 vibrational state and, accordingly, maximizes the change in absorption for the $v=2\rightarrow3$ transition. The ratio of the $v=1\rightarrow2$ to $v=2\rightarrow3$ absorption band intensity maxima gives a crude estimate for the relative initial population ratio produced by the three excitation pulses: the positive-chirped pulse has a 10:1 ratio, the near transform limited pulse ratio is 5:1 while the negatively-chirped pulse produces nearly equal intensity absorption bands. Similar quality data were obtained for several runs and the average of 4 of those runs produced each of the panels in Figure 3.

To better understand the effect of chirped-pulse excitation on the measured transient IR spectra portrayed in Fig. 3, density matrix theory was used to simulate population ladder climbing. Figure 4 shows the relative population depletion of the v=0 ground state by positively-chirped, transform-limited and negatively-chirped excitation pulses as a function of peak Rabi frequency. From experimentally known pump-pulse parameters, we calculate that the peak Rabi frequency corresponds to approximately 10 cm^{-1} in each case. Since the model does not include varying pulse amplitude or radial intensity averaging, we estimate that the effective Rabi frequency for the three pump pulses is about one-half of the peak value or 4-6 cm^{-1}. We find that the model predicts approximately 20-40% of the ground-state population is removed by both chirped excitation pulses. Interestingly, this depletion value is very close to the measured transient difference bleach intensity (typically ranging from OD=0.15 to OD=0.20 or 29%

to 37% excited species) giving us confidence that the model reasonably approximates the experimental conditions.

Figure 5 depicts the predicted v=1 excited state populations for the three types of pulses. The model indicates that the highest v=1 population should occur for the positively-chirped pulse while for the negatively-chirped case, it should be somewhat less (about 5%). This result is only qualitatively born out in the results of Fig. 3 which indicate that much higher v=1 excitation (absorption at 1968 cm^{-1}) is produced for the positively-chirped case compared to the negatively chirped case.

In Figure 6 we display the estimated relative population in v=2 created by the different pumping schemes. The model clearly predicts that v=2 population produced by negatively-chirped pulses should exceed (by ca. 3:1) that produced by the positively chirped excitation. The observation of substantially reduced $v=1\rightarrow2$ transient absorption (which could arise from excess population in the v=2 level since the intensity is proportional to the difference in v=1 and v=2 populations) and the clear enhancement in the $v=2\rightarrow3$ absorption at 1950 cm^{-1} (even after partial population relaxation to the v=1 level) strongly indicates that negatively-chirped IR excitation does indeed generate enhanced population in the v=2 excited state. It should also be noted that the predicted relative v=2 population might lie in the 5-10% range whereas excitation with positive pulses would produce at most a few percent absorption. This result can be compared to the measured $v=2\rightarrow3$ transient absorption change of ca. 0.02 OD (or 5% of the excited species occupy the v=2 level, assuming all transitions have similar oscillator strength and bandwidths). Finally, the model estimates the excited state population in v=3 to be 0.01% or less which is far below our detection limit of about 0.5% transmission change.

We emphasize that the model calculations as presented here should serve only as a guide for the interpretation of the experimental results. Although most of the qualitative behavior can be explained using this model we find issues that still need to be resolved. One example is the change in $v=1\rightarrow2$ absorption for the positive and unchirped cases, where we find experimentally that the unchirped pulse produces a larger $v=1\rightarrow2$ absorption than that predicted by the model. The parameters used for the field were chosen to represent in a general sense the amplitude, phase, and spectrum of the experimentally measured quantities. In a future communication we intend to more fully explore the dependence of vibrational population transfer on different laser field parameters and also incorporating actual experimentally measured fields.

CONCLUSIONS

Excitation with chirped ultrafast IR pulses can lead to control of the population distribution within a complex condensed-phase polyatomic molecular vibrational manifold in the electronic ground state. The dynamics of higher energy overtones can now potentially be explored with even shorter, broader bandwidth chirped IR pulses to provide information about experimentally inaccessible regions of the ground state potential energy surface. We showed that the absorption of several photons to climb a vibrational manifold can be manipulated by imposing an appropriate phase or chirp on a picosecond mid-IR excitation pulse.

In the near future, phase and amplitude-shaped ultrafast IR pulses could become a new tool to study bond dissociation [22]. One possibility is the investigation of dissociation mechanisms of highly vibrationally excited metal-carbonyl complexes with appropriately chirped 5 μm pulses. Infrared photodissociation of gas phase $Cr(CO)_6$ has been achieved [23,24] via multiphoton IR absorption under conditions where a large unspecified and uncontrolled number (ca. 20) of photons were employed. Using tailored ultrafast pulses, however, similar sample vibrational manifolds could be interrogated to yield snap-shots of the ladder-climbing process until the dissociation limit is reached. This type of investigation would therefore generate a more comprehensive description of ground electronic state dissociation mechanisms and perhaps lead to coherent control of bond-specific photochemistry.

ACKNOWLEDGMENTS

We gratefully acknowledge Dr. Todd A. Heimer for his assistance in acquiring some of the transient IR spectra and Dr. Andrea Markelz for very insightful discussions. This work was supported by NIST Scientific and Technical Research Services internal funding. VDK was also supported by The University of California at Los Angeles, Department of Chemical Engineering.

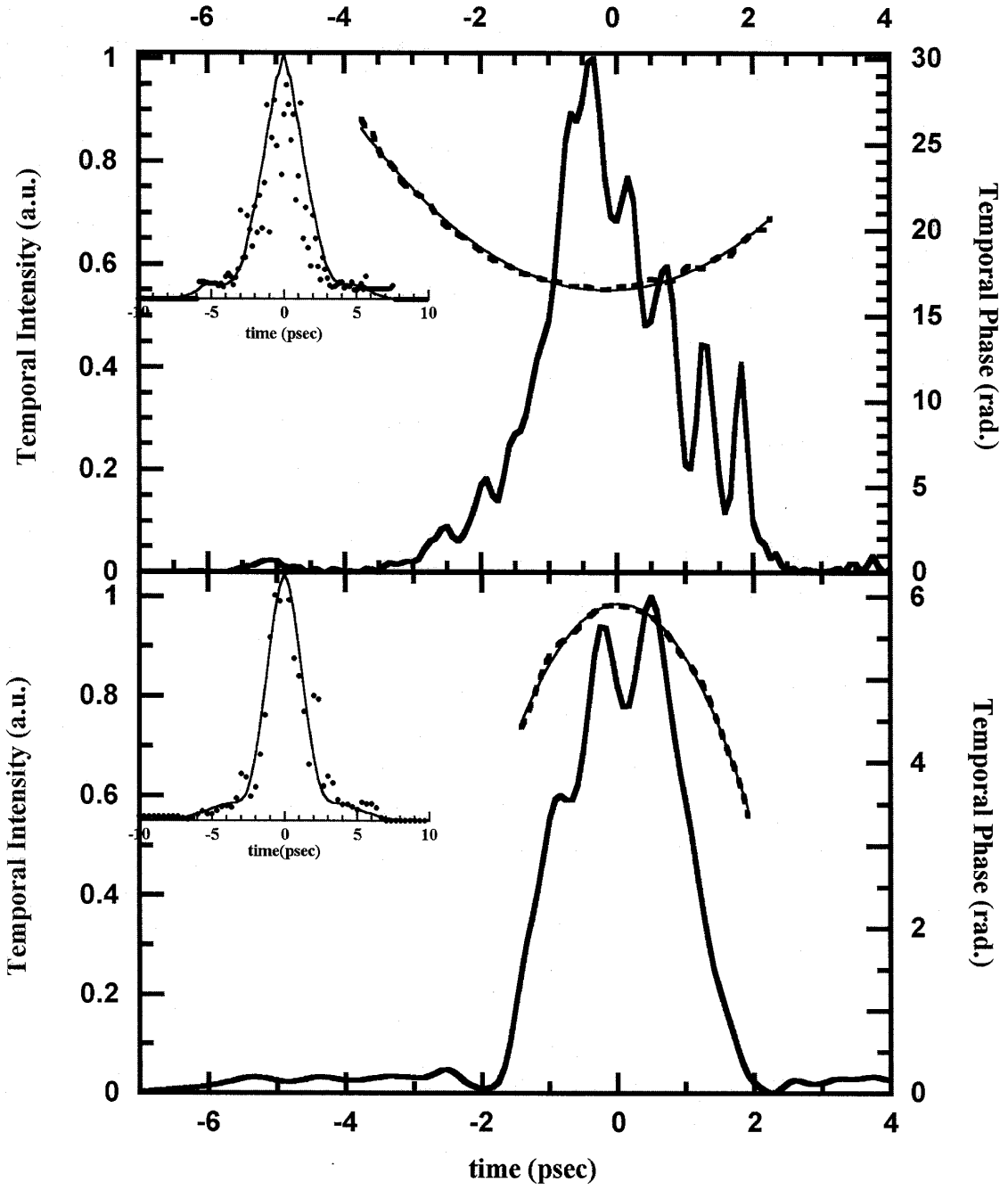

Figure 1. Retrieved SHG-FROG temporally-dependent intensities and phases of the negatively-chirped (top panel) and positively-chirped (lower panel) IR pulses used for up-pumping the T_{1u} CO-stretch manifold of $W(CO)_6$ in n-hexane. Quadratic fits (solid line) to the temporal phases (dashed line) yield –8 cm^{-1}/ps and +7cm^{-1}/ps chirp parameters, respectively. The insets in each panel correspond to the retrieved FROG autocorrelation function (squares) and the measured autocorrelation (solid line). See text for details.

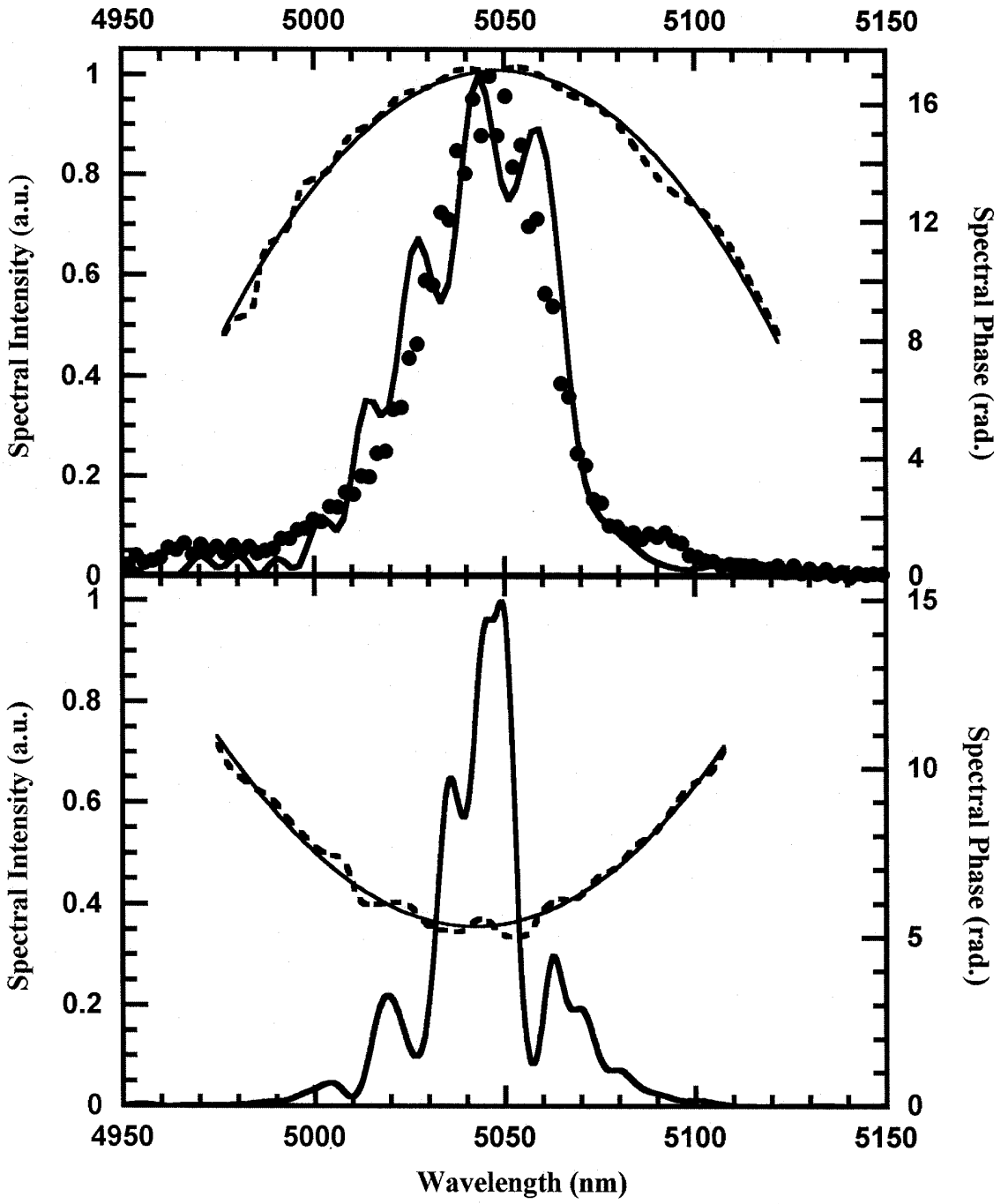

Figure 2. Retrieved SHG-FROG spectra and phases for the negatively chirped (top panel) and positively-chirped (lower panel) IR excitation pulses described in Fig. 1. An averaged spectrum obtained from a spectrograph-IR focal plane detector is given for comparison (top panel filled circles).

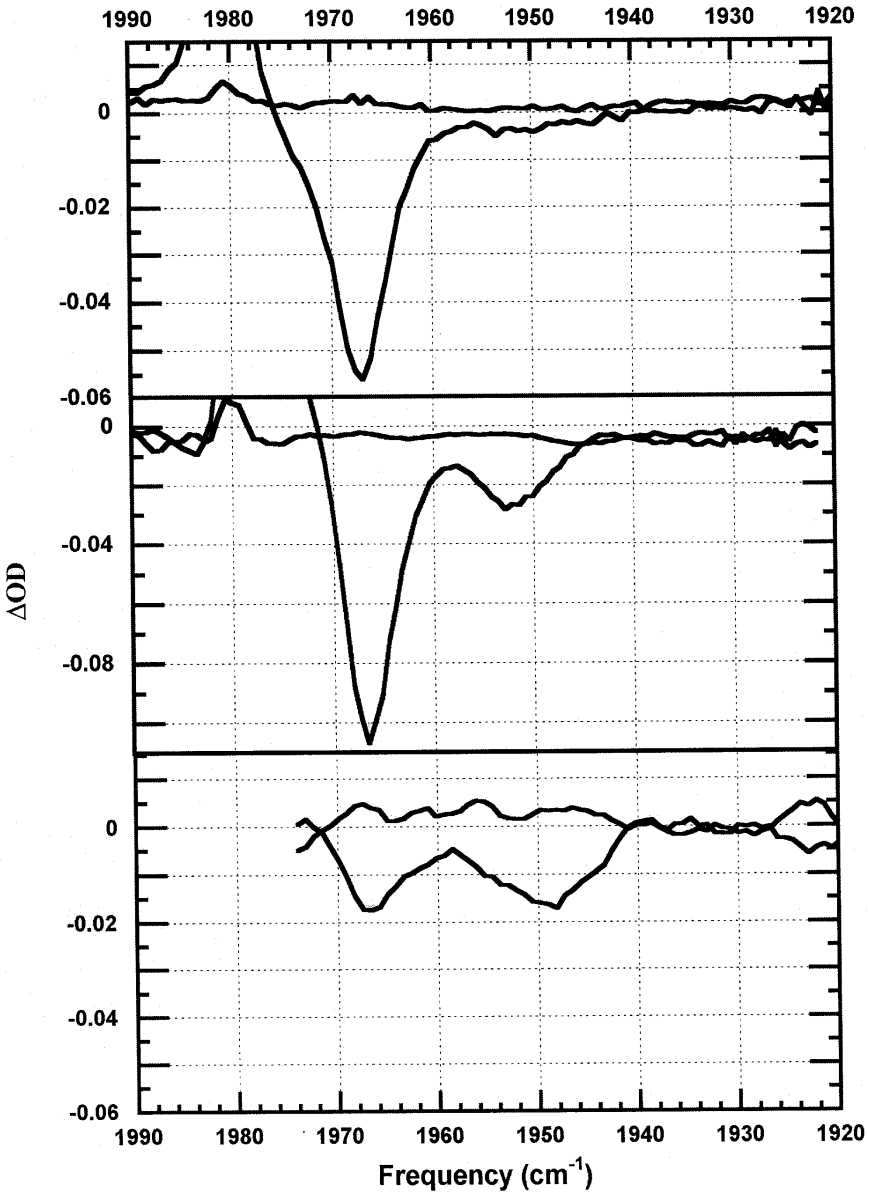

Figure 3. Infrared transient difference spectra for $W(CO)_6$ in room temperature n-hexane obtained at 40 ps time delay using ca. 2 ps positively-chirped (top), unchirped (middle) and negatively-chirped (bottom) excitation pulses centered near 1978 cm^{-1}. The promotion of excess v=2 population (absorption at 1950 cm^{-1}) relative to v=1 population by the negatively-chirped pulse is clearly evident.

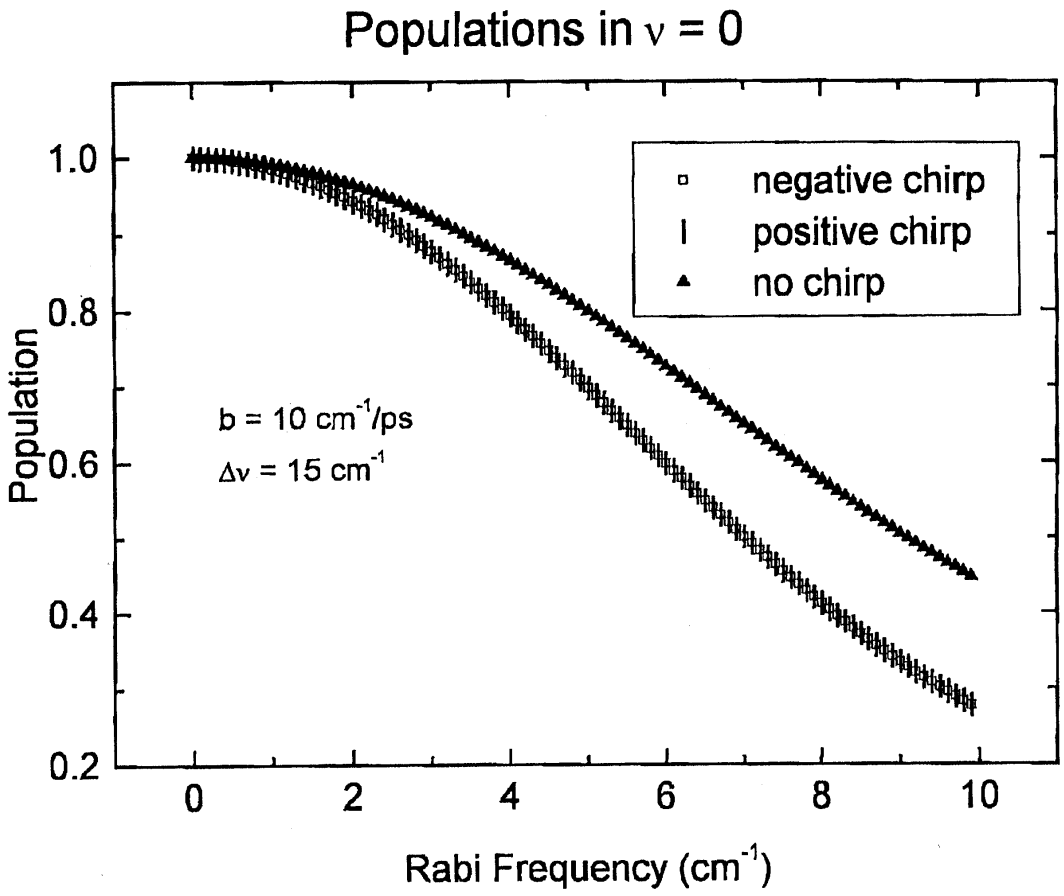

Figure 4. Model prediction of the relative v=0 ground state population remaining after excitation with chirped and unchirped infrared excitation as a function of peak Rabi frequency. Excitation pulse and molecular parameters used in this calculation are described in detail in the text.

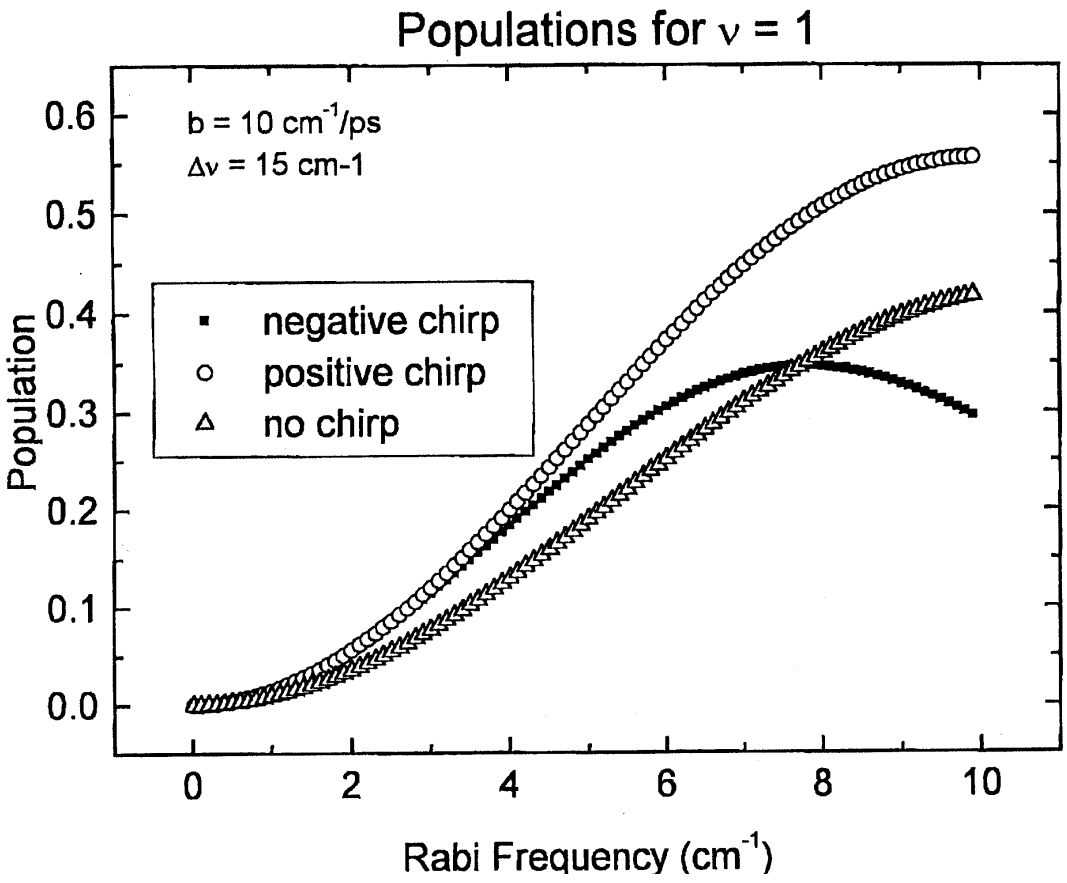

Figure 5. Relative v=1 excited populations predicted by the adiabatic model for different excitation pulse properties (see text).

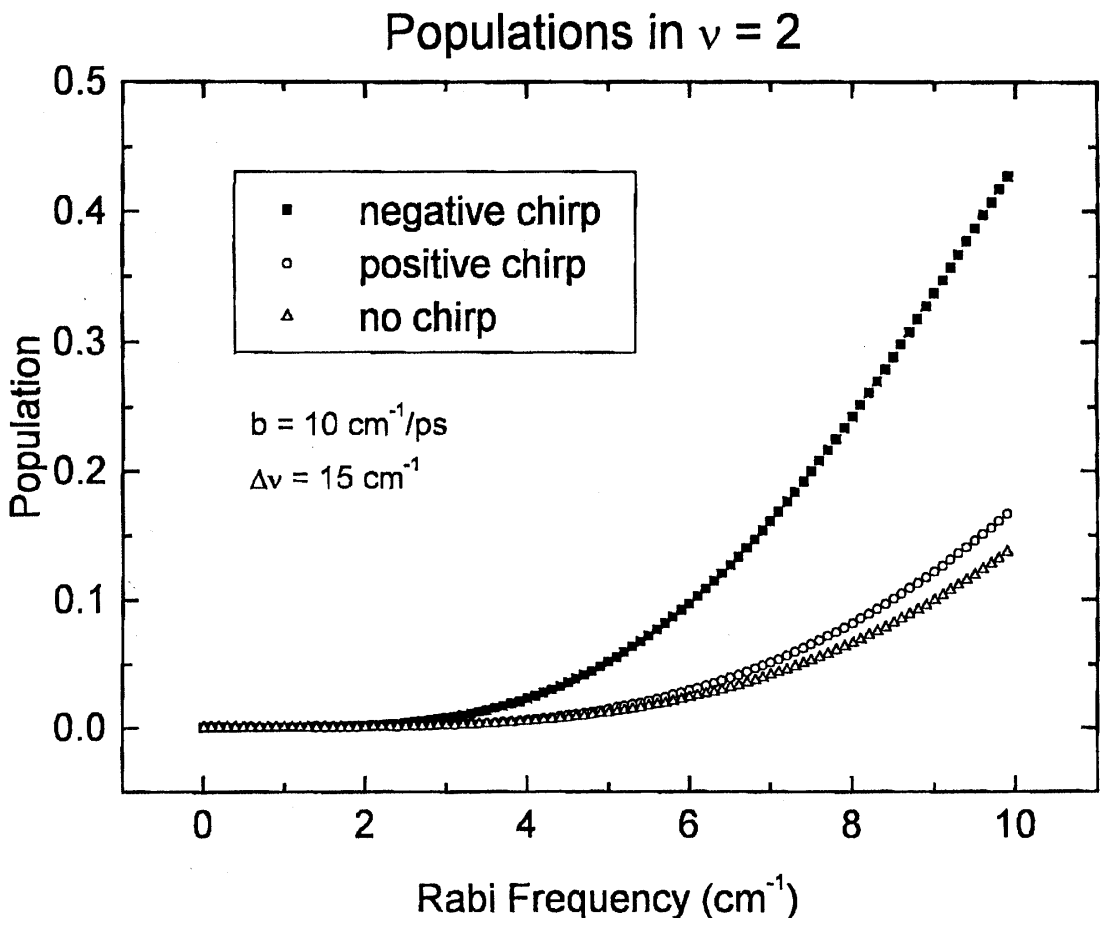

Figure 6. Modelled v=2 excited state populations for the same conditions described in Figs. 4 and 5. Excess v=2 population is expected when a negatively-chirped IR pulse is employed (see experimental result in Fig. 3).

REFERENCES

[1] S. Chelkowski, A. D. Bandrauk, Journal of Raman Spectroscpy 28 (1997) 459.

[2] B. Just, J. Manz, I. Trisca, Chem. Phys. Lett. 193 (1992) 423.

[3] M. V. Korolkov, J. Manz, G. K. Paramonov, J. Phys. Chem. 100 (1996) 13927.

[4] J. S. Melinger, D. McMorrow, C. Hillegas, W. S. Warren, Phys. Rev. A 51 (1995) 3366.

[5] G. K. Paramonov, Chem. Phys. 177 (1993) 169-180.

[6] C. J. Bardeen, Q. Wang, C. V. Shank, Phys. Rev. Lett. 75 (1995) 3410.

[7] S. Ruhman, R. Kosloff, Journal of the Optical Society of America B7 (1990) 1748.

[8] U. Gaubatz, P. Rudecki, S. Schiemann, K. Bergmann, J. Chem. Phys. 92 (1990) 5363.

[9] R. J. Gordon, S. A. Rice, Annual Reviews of Physical Chemistry 48 (1997) 601.

[10] B. Kohler, V. V. Yakovlev, J. W. Che, J. L. Krause, M. Messina, K. R. Wilson, N. Schwentner, R. M. Whitnell, Y. Yan, Phisical Review Letters 74 (1995) 3360.

[11] C. J. Bardeen, J. W. Che, K. R. Wilson, V. V. Yakovlev, V. A. Apkarian, C. C. Martens, R. Zadoyan, B. Kohler, M. Messina, J. Chem. Phys. 106 (1997) 8486.

[12] S. H. Ashworth, T. Hasche, M. Woerner, E. Riedle, T. Elsaesser, J. Chem. Phys. 104 (1996) 5761.

[13] P. Balling, D. J. Maas, L. D. Noordam, Phys. Rev. A 50 (1994) 4276.

[14] B. Borers, H. B. van Linden van den Heuvell, L. D. Noordam, Phys. Rev. Lett. 69 (1992) 2062.

[15] D. J. Maas, D. I. Duncan, A. F. G. van der Meer, W. J. van der Zande, L. D. Noordam, Chem. Phys. Lett. 270 (1997) 45.

[16] S. M. Arrivo, T. P. Dougherty, W. T. Grubbs, E. J. Heilweil, Chem. Phys. Lett. 235 (1995) 247.

[17] S. M. Arrivo, V. D. Kleiman, T. P. Dougherty, E. J. Heilweil, Opt. Lett. 22 (1997) 1488.

[18] J.-C. Diels, W. Rudolph. Ultrashort Laser Pulse Phenomena; Academic Press, Inc.: San Diego, CA, 1996; pp 343.

[19] M. M. Choy, R. L. Byer, Physical Review B 14 (1976) 1693.

[20] D. J. Kane, R. Trebino, IEEE Journal of Quantum Electronics 29 (1993) 571.

[21] A. Tokmakoff, B. Sauter, A. S. Kwok, M. D. Fayer, Chem. Phys. Lett. 221 (1994) 412.

[22] S. Chelkowski, A. D. Bandrauk, P. B. Corkum, Phys. Rev. Lett. 65 (1990) 2355.

[23] S. A. Trushin, K.-i. Sugawara, H. Takeo, Chem. Phys. 203 (1996) 267.

[24] M. B. Knickelbein, J. Chem. Phys. 104 (1995) 3517.